Quantitative Structural Activity Relationship (QSAR), Density Functional Theory (DFT), Molecular Docking, ADMET and Target Prediction Studies of Antimalarial activity of 1,2,4-triazolo[4,3-a]pyrazine derivatives against Resistant *Plasmodium Falciparum*

Olatunji Nathaniel Oladoye[1], Oladuji Tofunmi Emmanuel[1], Olatunde Abimbola Modupe[2], Asibor Yemisi Elizabeth [3]and Semire Banjo[1]*

[1]Department of Pure and Applied Chemistry, Faculty of Pure and Applied Sciences, Ladoke Akintola, University of Technology, P.M.B-4000, Ogbomosho, Oyo State, Nigeria
[2]Department of Chemistry, University of Ibadan, Ibadan. Oyo State, Nigeria
[3]Osun State University, Department of Pure & Applied Chemistry, Osogbo, Nigeria.
*Corresponding e-mails: bsemire@lauctech.edu.ng
DOI: 10.56201/ijccp.v10.no5.2024.pg65.91

Abstract

Quantum Chemical Methods via Density Functional Theory (DFT), Quantitative Structure Activity Relation (QSAR) and docking methods were used to observed the anti-malaria activity of 1,2,4-triazolo[4,3-a] pyrazine derivatives. Many descriptors including dipole moment (DM), hydrogen bond donor (HBD), hydrogen bond acceptor (HBA), highest occupied molecular orbital (HOMO), lowest unoccupied molecular orbital (LUMO), hydrophobicity (LogP), energy gap (ΔEg), chemical hardness (η), softness, and chemical potential (μ) energies were calculated. All the five QSAR models were validated and the results showed that R-squared (R^2), adjusted R² (R²adj), cross-validation (Q²), standard error of estimation (SEE) and mean absolute error (MAE) ranged from 0.9457 – 0.9902, 0.9225 – 0.9861, 0.8917 – 0.9789, 0.0687 – 0.1621, and 0.0676 – 0.01190, respectively, indicating that all the models have good predictability. However, models 1 (with R^2 = 0.9902, R²adj = 0.9861, Q² = 0.9789, SEE = 0.0687 and MAE = 0.0676) was used to predict new set of triazolo[4,3-α] pyrazine due to its statistical robustness. The docking results of the six predicted triazolo[4,3-α] pyrazine compounds (NLs) and the standard drugs (Artesunate, Puromycin, and Pyrimethamine) against Plasmodium falciparum (PfMyoA) with PDB ID 6YCX, 6YCY, and 6YCZ revealed the binding affinities range of -7.80 to -9.30 kcal/mol for 6YCX, -7.60 to -9.30 kcal/mol for 6YCY and -7.90 to -9.00 kcal/mol for 6YCZ. The binding affinities of Artesunate, Puromycin and Pyrimethamine are -7.70, -7.90 and -6.60 kcal/mol for 6YCX, -7.50, -8.20 and -6.40 kcal/mol for 6YCY, -8.00, -8.30 and -6.70 kcal/mol, respectively, indicating that NL7, NL8, NL9, NL10 and NL18 have outstanding binding affinity than the selected drugs. The ADMET profiles, the computational QSAR study together with the molecular docking has actually provided a valuable approach for researchers to developed model, making it possible to predict the bioactivities of the related ligands. Therefore, molecular docking studies showed that there is presence of hydrogen bond interaction of the ligands with the amino acid residue in the binding site of the receptor. Conformation of the ligands was significant features for the ligand-receptor binding. Serious investigation and correlation among binding affinity and IC$_{50}$ revealed that, the ligand in the active site is better than standard drugs.

Keywords: *1,2,4-triazolo[4,3-a] pyrazine derivatives, DFT-QSAR, Molecular docking*

1.0 Introduction

Malaria is frightening disease transmitted to humans through the bites of infected female Anopheles mosquitoes [1]. The disease is caused by single-celled parasites of the genus Plasmodium; these mosquitoes become infected by feeding on a person already carrying the malaria parasites, which they then transmit to another person. Once inside the human body, the parasites travel to the liver, reproduce, and spread. Malaria becomes symptomatic when the parasites mature, leave the liver, and infect red blood cells [2]. It can also be transmitted through blood transfusions or shared needles used by an infected person [3]. Mild symptoms of malaria include fever, tiredness, vomiting, and headaches. Severe cases, particularly those caused by Plasmodium falciparum, can lead to yellow skin, seizures, coma, or death. Mild symptoms typically appear ten to fifteen days after infection, and if untreated, the condition may worsen. The risk of the disease can be reduced by preventing mosquito bites using mosquito nets and insect repellents, draining standing water, and spraying insecticides [4]. In 2019, 229 million people worldwide were infected with malaria, with a mortality rate of 409 thousand [1]. As of 2020, there is one vaccine that has been shown to reduce the risk of malaria by 40% in children. Despite advances, treating malaria remains a challenge for medical researchers and practitioners. Treatment often involves a combination of antimalarial medications such as artemisinin paired with lumefantrine, mefloquine, or sulfadoxine/pyrimethamine. In cases where artemisinin is unavailable, quinine combined with doxycycline may be used [5]
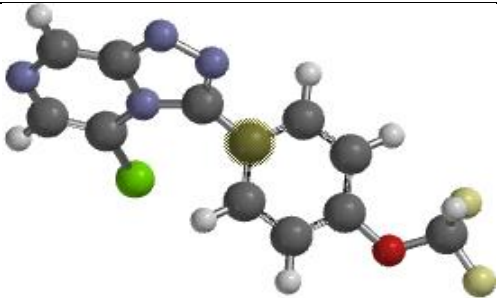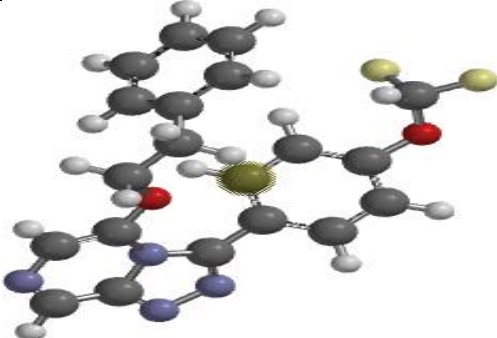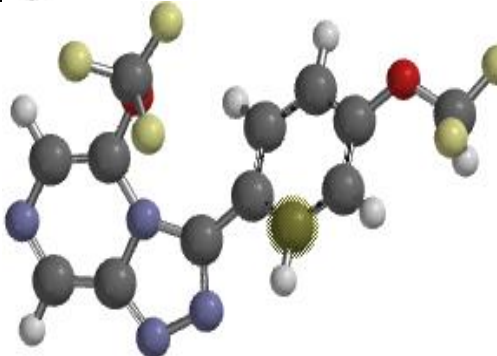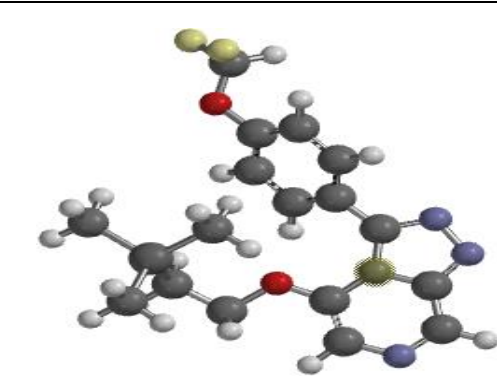
Antimalarial drug resistance can be, the ability of a parasite strain to survive or multiply despite the administration and absorption of medication given in doses equal to or higher than those usually recommended, provided that drug exposure at the site of action is adequate. Resistance arises from the selection of parasites with genetic mutations or gene amplifications that confer reduced susceptibility [6]. The chemistry of heterocyclic molecules plays a critical role in developing effective drugs for treating bacterial and viral diseases [7]. These molecules are present in both synthetic and natural compounds used for malaria treatment. Triazole derivatives are used as sedatives [8] anti-inflammatory agents [9] anti-migraine drugs [10] antiviral agents [11] and antimalarial agents [12]. Pyrazine derivatives, which are two-nitrogen-containing six-membered ring aromatic heterocyclic compounds, can carry substituents at one or more of the four ring carbon atoms [13].
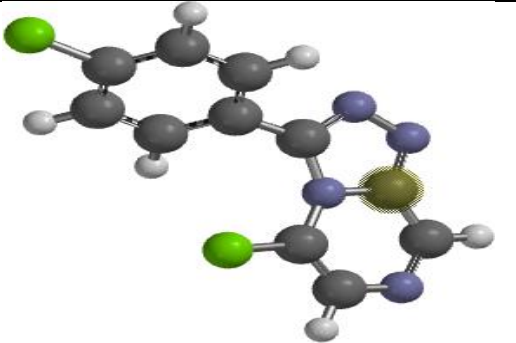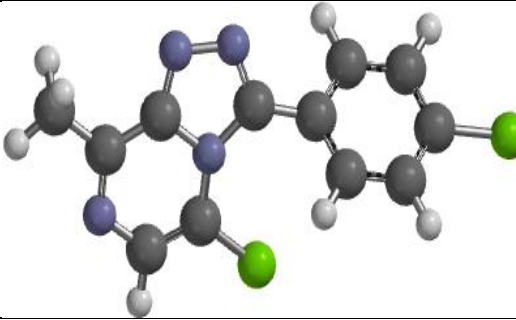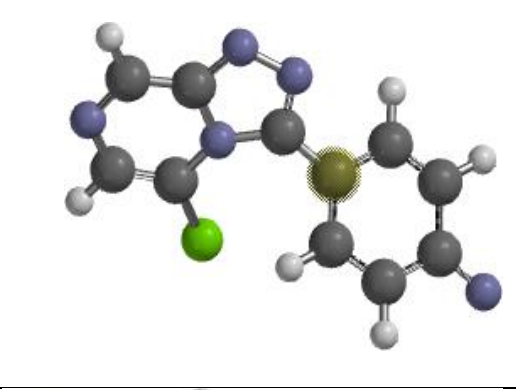
Pyrazines occur naturally and can be synthesized by various methods. They possess diverse pharmacological properties, including antibacterial, antifungal, antimycobacterial, anti-inflammatory, analgesic, anticancer, antidiabetic, arteriosclerosis treatment, and antiviral activities [14].Also, sequences of 1,2,4-triazolo[4,3-a] pyrazine scaffolds were synthesized and demonstrated potency down against the malaria parasite *Plasmodium falciparum* (*Pf*) and appears to have little poly-pharmacology or cytotoxicity, giving confidence in its acceptability, making it ideal for a targeted medication [15]. Completely compounds tested for their ability to inhibit the growth of the malaria parasite *Plasmodium falciparum* (3D7 and Dd2 strains) and for cytotoxicity against a human embryonic kidney (HEK293) cell line. Reasonable antimalarial activity was observed for some of the compounds, with IC50 values ranging from 0.3 to >20 µM; none of the compounds displayed any toxicity against HEK293 at 80 µM.
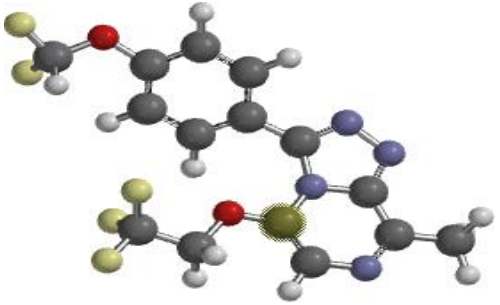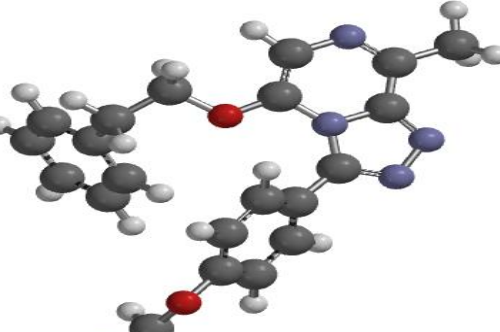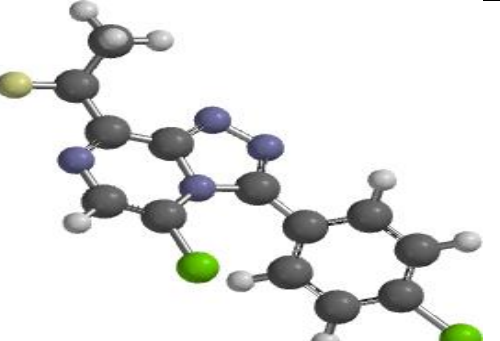
Furthermore, in this research*, in-silico* methods would be used for further investigations of 1,2,4-triazolo[4,3-a] pyrazine hybrids conducted by Johnson et al. [16] as outlined in Table 1. Though, this would, stress on the development of robust QSAR using multiple linear regression-Genetic Algorithm (MLR-GA) to propose new set of new triazolo-pyrazine hybrids
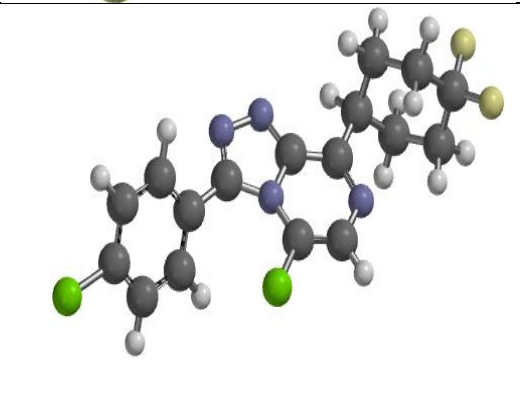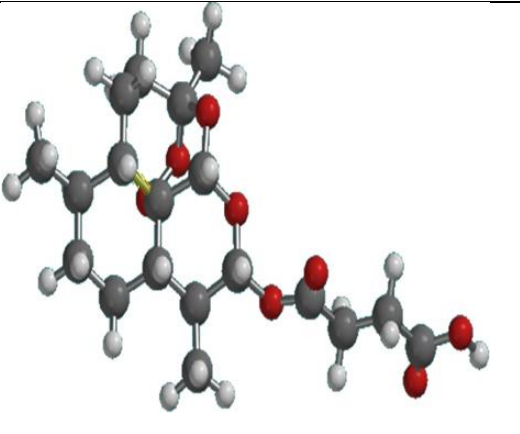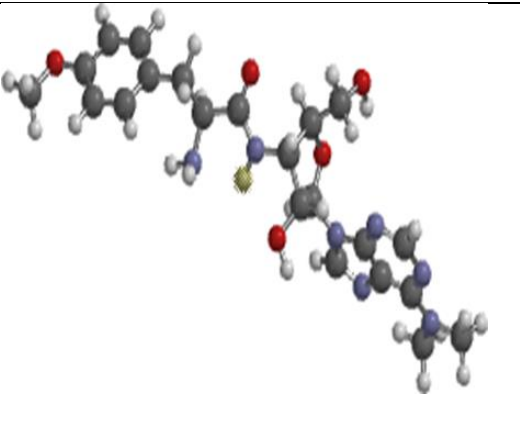
with improved Antimalarial activity against *Plasmodium falciparum* myosin A (6YCX,6YCY, and 6YCZ). Hence, the aim of this work is to develop robust QSAR model, designed novel triazolo-pyrazine hybrids, predict their inhibitory properties and molecular docking analysis.
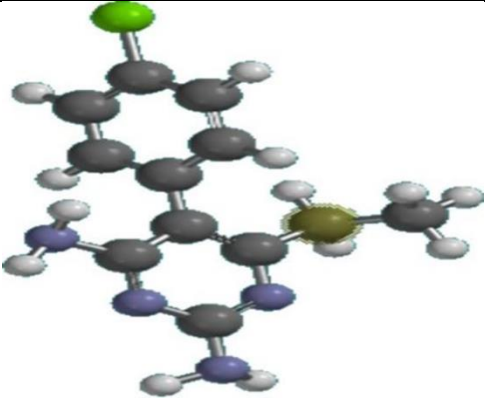
Table: 1 Structures, IUPAC Names and **IC$_{50}$**

Ligands	Structure	IUPAC Name	IC$_{50}$
LI		3-[4-(Difluoromethoxyl) phyenyl]-5-(2-phenylethoxy) [1,2,4] triazolo[4,3-α] pyrazine.	16.81
L2		3-[4-(Difluoromethoxyl) phyenyl]-5-(2-phenylethoxy) [1,2,4] triazolo[4,3-α] pyrazine.	0.31
L3		3-[(4-(Difluoromethoxy) phyenyl]-5-(2,2,2-trifluroethoxy)- [1,2,4] triazolo[4,3-α] pyrazin	16.65
L4		3-[4-(Difluoromethoxy) phyenyl]-5-(2-trimethlsilyl) ethoxy]- [1,2,4] triazolo [4,3-α] pyrazine	13.86

L5		5-Chloro-5-(2-Chrolophenyl)-8-methyl [1,2,4] triazolo [4,3-α] pyrazine	12.62
L6		5-Chloro-3-(4-Chlorophenyl)-8-methyl-1,2,4-triazolo [1,2,4] triazolo [4,3-α] pyrazin-3yl benzonitrile	19.18
L7		4-(5-Chloro-5-methyl-1,2,4-trizolo 4,3-a] pyrazin-3-yl) benzonitrile	18.89
L8		4-(5-Chloro-8-methyl-1,2,4-trizolo 4,3-a] pyrazin-3-yl) benzonitrile	27.33
L9		5-chloro-3-[4-Difluoromethoxy] phenyl-8-methyl- [1,2,4] triazolo [4,3-α] pyrazine	12.49

L10		3-[4-Difluoromethoxy] phenyl-8-methyl-5-(2,2,2-trifloroethoxy)-[1,2,4] triazolo [4,3-α] pyrazine	27.33
L11		3-[4-Difloromethoxy] phenyl-8-methyl-5-(2-phenylethoxyl)-[1,2,4] triazolo [4,3-α] pyrazine	11.01
L12		5-chloro-3-[4-Chlorophenyl]-8-(1,1-trifluoromethyl)- [1,2,4] triazolo [4,3-α] pyrazine	4.84
L13		5-chloro-3-[4-Chlorophenyl]-8-(1,1-difluoroethyl)- [1,2,4] triazolo [4,3-α] pyrazine	1.72

L14		3-(4-chlorophenyl)-8- [1,1-difluoro ethyl]- [1,2,4] triazolo [4,3-α] pyrazine	6.40
L15		5-chloro-3-[4-Chlorophenyl]-8-(4,4-difluorocyclohexyl)- [1,2,4] triazolo [4,3-α] pyrazine	20.19
16		Artesunate	3.48
17		Puromycin	95.28

| 18 | | pyrimethamine | 12.08 |

2.0 Methods of *In-silico*

A set of fifteen triazolo- pyrazine hybrids and commercially available drugs were gotten from the work of Johnson et al. [16] as revealed in Table 1. The biological activity of the ligands was expressed as concentration (IC_{50}). The IC_{50} values were subjected to conversion data by taking to the negative logarithm of base 10 according to the equation:

$$pIC_{50} = -\log(IC_{50} \times 10^{-6}) \qquad 1$$

Then, the ligands were subjected to optimized using the density functional theory (DFT) method for molecular geometries Spartan 14 software as described [17] and various molecular descriptors were calculated, including dipole moment (DM), hydrogen bond donor (HBD), hydrogen bond acceptor (HBA), highest occupied molecular orbital (HOMO), lowest unoccupied molecular orbital (LUMO), hydrophobicity (LogP), energy gap (ΔEg), chemical hardness (η), softness, and chemical potential (μ) energies. [18].

2.1 Modelling of QSAR

The optimized structures were transformed into Spatial Data File *sdf format to create molecular descriptors using the Padel-Descriptor software [19]. This process formed over 1,200 descriptors based on 1D, 2D, and 3D parameters, including geometrical and topological descriptors. The dataset was randomly divided into a training set (70%) for developing the Quantitative Structure-Activity Relationship (QSAR) model and a test set (30%) for model validation. The QSAR model utilized compounds from both sets, correlating the independent variables (descriptors) with the dependent variable. Validation of the QSAR models confirmed their internal stability and predictive accuracy through both internal and external validation methods [20-21]. Cross-validation assesses the reliability of a QSAR model in estimating the prognostic control and is estimated using equation 2

$$\mathrm{CV.R}^2 = 1 - \frac{\Sigma(\mathrm{YObs-YCal})^2}{\Sigma(\mathrm{YObs-YObs})^2} \qquad 2$$

$$R_a^2 = \frac{(N-1) \, x \, R^2 - P}{N-1-P} \qquad 3$$

where N= number of compounds in the training set, R^2 is the correlation coefficient, P= number of the descriptor in the model, and N -1- P is the degree of freedom

$$SEE = \sqrt{\frac{(Y_{exp} - Y_{pred})^2}{N-P-1}} \qquad 4$$

The Standard Error of Estimation (SEE) corresponds to the model's standard deviation, serving as a measure of model quality. A model with a lower SEE value is considered superior. SEE is determined by the equation provided above. Y_{exp} and Y_{pred} are set as concentration of the training set and test set respectively.

The characteristics of inter-correlated descriptor model are evaluated based on their multicollinearity estimated using the variation inflation factor (VIF) as shown in equation 5.

$$VIF = (1 - R^2)^{-1} \hspace{4cm} 5$$

2.2 Docking of the Target Receptor Preparation

The Protein ID: 6YCX, 6YCY, and 6YCZ were retrieved from the Protein Data Bank (PDB) RCSB (http://www.rcsb.org/pdb). Pymol and Discovery Studio Software facilitated the preparation of the receptor by removing water molecules, cofactors, and other unwanted entities, thereby preventing molecular interactions during virtual screening [22]. These prepared receptors were saved in the PDB file format and molecular docking was performed using PyRx software; the docking results were analysed with Discovery Studio Software

3.0 Result and Discussion
3.1 Modelling QSAR using Multilinear Regression Genetic Algorithm (MLR-GFA)

The study on the antimalarial activity of triazolo[4,3-a] pyrazine hybrids and selected antimalarial drugs targeting the Plasmodium falciparum's Myosin A, as reported by Johnson et al. [16], was used for QSAR modelling. QSAR (Quantitative Structure-Activity Relationship) correlates the structural properties of compounds with their biological activities. This study evaluated fifteen (15) compounds, excluding one outlier, with eleven (10) compounds serving as the training set and the remaining four (4) as the test set. Descriptors or specific parameters were automatically selected using Genetic Algorithms and Linear Discriminant Analysis (GA-LDA) to minimize multi-collinearity. Five models were developed, with symbols definitions and descriptors used in the MLR-GFA (Multiple Linear Regression-Genetic Function Approximation) equation as revealed in Table 2 and 3. Among the five models developed, Model 1**:** The QSAR model was built and statistically validated.

Table 2 highlighted the significant positive contribution of MDEC-22 (Molecular Distance Edge between all secondary carbons) and the lesser but still significant negative contributions of WTPT-2 (Molecular ID/number of atoms) and SpMax5_Bhp (Largest absolute eigenvalue of Burden modified matrix - n5/weighted by relative polarizabilities) for model 1.These models were separately statistically validated using metrics such as R-squared (R^2), adjusted R^2, Cross-validated R^2 (Q^2), Standard Error of Estimation (SEE), Q^2(LOO) (Leave-One-Out Cross-Validation), SDEP(LOO) (Standard Deviation Error of Prediction), Scaled average Rm²(LOO), Scaled delta Rm²(LOO), Mean Absolute Error (MAE), and Prediction Quality (MAE-based criteria) as shown in Table 4. The experimental pIC50 and predicted pIC50 values are displayed in Table 5. The Pearson correlation analysis indicated that the selected descriptors used for developing model 1 are non-collinear, with MDEC-22 significantly contributing to pIC50 Table 6. The residual values observed between the experimental and predicted pIC50 further validated the model's reliability.

Figure 1a presented a plot of the predicted pIC50 versus experimental pIC50 for the compounds, showing that the predicted values closely align with the experimental values, confirming the model's dependability. Additionally, figure 1b displayed a scatter plot of residuals against the experimental pIC50, providing further evidence

.   **Table 2:** QSAR validation parameters.

MODEL 1	pIC50 = 41.1149 -15.541* WTPT-2 - 4.3023* SpMax5_Bhp + 0.2922* MDEC-22
MODEL 2	pIC50 = 1.8672 + 4.4844 * MATS1i -3.8504* SpMin5_Bhs + 0.2236*MDEC-22
MODEL 3	pIC50 = 0.1907- 0.267* MDEC-23 + 0.1031* nX + 0.329* MDEC-22
MODEL 4	pIC50 = -0.7646 + 0.0083* AATS7m + 0.305* MDEC-22 - 0.2204*MDEC-23
MODEL 5	pIC50 = 1.8183 - 1.2979*GATS1i + 0.294*MDEC-22 - 0.243* MDEC-23

Table 3   Symbols definitions and descriptors used in the MLR-GFA equation.

S/N	Descriptor	Definition	Class	Contribution
1	WTPT-2	Molecular ID / number of atoms	2D	Negative
2	SpMax5_Bhp	Largest absolute eigenvalue of Burden modified matrix - n 5 / weighted by relative	2D	Negative
3	MDEC-22	Molecular distance edge between all secondary carbons	2D	Positive

Table 4: QSAR validation parameters.

S/N	Parameter	Threshold Value	MODEL 1	MODEL 2	MODEL 3	MODEL4	MODEL 5	STATEMENT
1	R-squared (R^2)	> 0.6	0.9902	0.9457	0.9778	0.9841	0.9849	GOOD
2	Adjusted R^2 (R^2adj)	> 0.6	0.9861	0.9225	0.9682	0.9773	0.9785	GOOD
3	Cross validated R squared (Q^2)	> 0.5	0.9789	0.8917	0.9265	0.9655	0.9473	GOOD
4	$VIF = (1 - R^2)^{-1}$	< 6	0.0098	0.0543	0.0222	0.0159	0.0151	GOOD
5	R^2 - Q^2 LOO	< 0.3	0.0113	0.0540	0.0513	0.0186	0.0376	GOOD
6	Standard Error of Estimation (SEE)	0.5	0.0687	0.1621	0.1037	0.0876	0.0854	GOOD
7	SDEP (LOO)	0.6	0.0806	0.1826	0.1504	0.1031	0.1274	GOOD
8	Scaled average Rm^2(LOO)	0.88	0.9719	0.8578	0.9031	0.955	0.9243	GOOD
9	Scaled delta Rm^2	0.5	0.0111	0.0256	0.0463	0.0139	0.0336	GOOD
10	Mean Absolute Error (MAE)	< 1	0.0676	0.1603	0.119	0.0876	0.113	GOOD

Table: 5 The experimental and predicted pIC_{50} of the ligands for model 1

Ligand	Experimental pIC$_{50}$ (μM)	Predicted pIC$_{50}$ (μM)	Residual
M1	-1.22557	-1.25396	0.028393
M2	0.508638	0.492213	0.016426
M3	-1.22141	-1.1176	-0.10382

M4	-1.10106	-1.09834	-0.00272
M5	-1.28285	-1.20341	-0.07944
M6*	-1.27623	-1.09834	-0.17789
M7*	-1.43664	-1.51151	0.07487
M8*	-1.09656	-1.74317	0.646613
M9	-1.43664	-1.4365	-0.00014
M10*	-1.04179	-1.16085	0.119068
M12	-0.68485	-0.7690	0.084155
M13	-0.23553	-0.17935	-0.05618
M14	-0.80618	-0.83623	0.030054
M15	-1.30514	-1.35844	0.053303

*The predicted values for test data

Table 6: Pearson correlation for Model 1

	pIc50	WTPT-2	SpMax5_Bhp	MDEC-22
pIc50	1			
WTPT-2	-0.36053	1		
SpMax5_Bhp	0.195989	0.194618	1	
MDEC-22	-4.8E-05	0.561272	0.81927	1
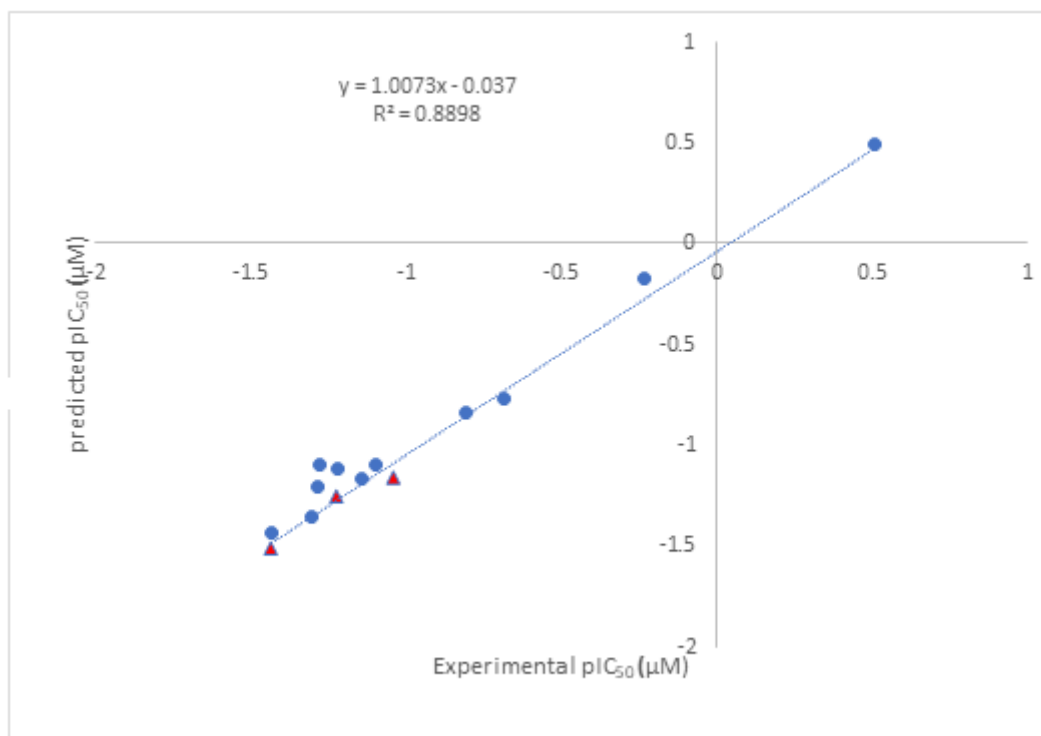
Figure 1a: Plot of observed and predicted pIC50
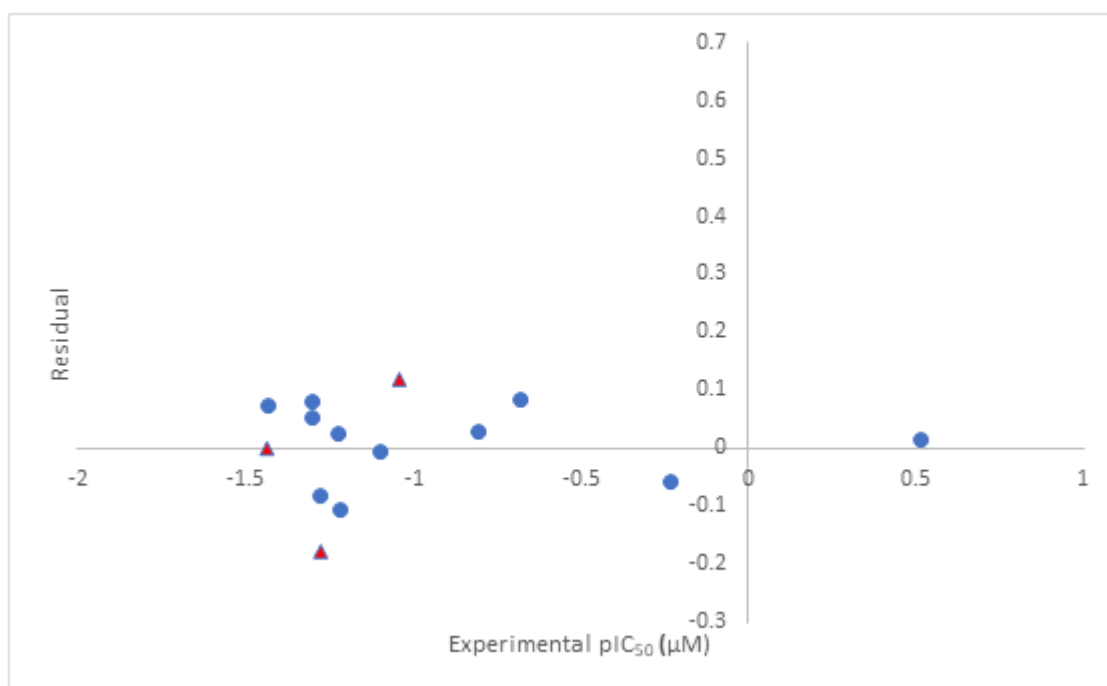
Figure 1b: Residual plot against observed pIC50

3.2 The frontier energies and chemical reactivity descriptors of Proposed 1,2,4-Triazolo [4, 3-a] Pyrazine Hybrids

Twenty new 1,2,4-triazolo[4,3-a] pyrazine hybrids or derivatives based on L2 (Table 1) from experimental data [16] were subjected to optimization using the Density Functional Theory (DFT.B3LYP.6-31G**) method (Figure 2). The molecular descriptors were calculated from the ground state optimized geometries as related to the bioactivity of the compounds.
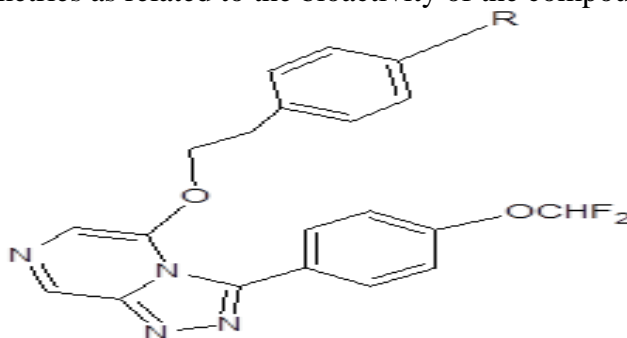
NL1: R = CH$_3$ NL2: R = OCH$_3$ NL3: R = Cl   NL4: R = F

NL5: R = OH   NL6: R = NO$_2$ NL7: R = CH$_2$F   NL8: R = OCH$_2$F

NL9: R = CF$_3$ NL10: R = OCF$_3$ NL11: R = Br   NL12: R = ON

NL13:   R   =   NL14: R = SH   NL15: R = CH$_2$CH$_3$ NL16: R = CH$_2$OH
CH$_3$CH$_2$Br

NL17: R = CH$_2$CH$_5$ NL18:   R   =   NL19: R = CH$_2$Cl$_5$ NL20: R = N(CH$_3$)$_2$
                              CH$_2$COOH

Figure 2: proposed new trizole-pyrazine hybrids from 3-[4-(Difluoromethoxyl) phyenyl]-5-(2-phenylethoxy) [1,2,4] triazolo[4,3-α] pyrazine

The calculated HOMO energies for the compounds and standard drugs were -6.68, -6.50, -6.39, -6.45, -6.47, -6.56, -6.54, -5.74, and -5.65 eV for NL7-NL10, NL18, NL19, Artesunate, Puromycin, and Pyrimethamine, respectively (Table 2). NL7 has the highest HOMO energy value at -6.56 eV, indicating a higher ability to donate electrons to neighbouring compounds/receptors among the new compounds, but not as high as the standard drugs [20]. Similarly, the LUMO values indicated that all the new compounds have lower LUMO energies than the standard drugs. However, the LUMO energies of NL19, NL8, and NL7 suggest they have a higher probability of accepting electrons [20]. Moreover, the LogP values revealed that NL7-NL10 and NL19 could pass through cell membranes more easily than the standard drugs. The energy gap (ΔEg = 3.22 eV), chemical hardness (1.61 eV), and softness (0.621 eV) Favor interactions of NL19 with proteins over the standard drugs [23-24].

Table 6: **The calculated molecular descriptors obtained from the studied compounds**

S/N	E_{HOMO}	E_{LUMO}	OVAL	HBA	HBD	Chemi potential (μ)	Chemi soft	Chemi Hardnes η (eV)	Band gap ΔEg	LOGP	ω (eV)	DM	IC50
NL7	-6.68	-2.07	1.60	5	0	- 4.61	0.220	2.31	4.38	5.50	4.41	6.48	0.46
NL8	-6.50	-2.01	1.62	6	0	- 4.23	0.445	2.25	4.49	5.20	3.98	7.42	0.39
NL9	-6.39	-1.98	1.59	5	0	- 4.19	0.454	2.21	4.41	5.50	3.97	8.23	0.34
NL10	-6.45	-1.98	1.58	5	0	- 4.22	0.447	2.24	4.47	6.07	3.97	7.19	0.44
NL18	-6.47	-2.03	1.61	6	1	- 4.25	0.450	2.22	4.44	4.74	4.07	9.73	0.40
NL19	-6.56	-3.34	1.58	7	0	- 4.95	0.621	1.61	3.22	5.19	7.61	7.71	0.77
ARTES	-6.54	0.15	1.54	6	1	-3.35	0.160	3.20	6.39	2.73	1.76	0.91	3.48
PURO	-5.74	-0.64	1.71	10	3	-3.19	0.190	2.55	5.10	2.88	2.00	7.29	95.28
PYRIM	-5.65	-0.59	1.41	2	0	-3.12	0.190	2.53	5.06	0.24	1.92	1.67	12.08

3.3 Docking results of Proposed 3-[4-(Difluoromethoxyl) phyenyl]-5-(2-phenylethoxy) [1,2,4] triazolo[4,3-α] pyrazine against *Plasmodium Falciparum* (6YCX)

The purpose of the docking study is to identify the conformation of compounds or ligands within the active site of a protein and to predict their binding affinities. The binding affinities for the new ligands ranged from -7.8 (NL19) to -9.3 kcal/mol (NL9), whereas the standard drugs showed binding affinities of -6.6 kcal/mol (pyrimethamine), -7.7 kcal/mol (artesunate), and -7.9 kcal/mol (pyrimethamine). This indicates that the new ligands are more bioactive antimalarials (Ki = 0.15 - 1.93 µM) compared to the standard drugs (Ki = 1.63 - 14.59 µM), as shown in Table 7. The receptor amino acids in the binding site forming hydrogen bonds with ligands (H-bond distance, Å) are also displayed in Table 7. Although many of these compounds exhibited good IC50 values, the best compounds were NL7 (0.46), NL8 (0.39), NL9 (0.34), NL10 (0.44), NL18 (0.40), and NL19 (0.77), which correspond with their calculated binding affinities.

NL9 interacted through Van der Waals forces, carbon-hydrogen bonds, halogen (fluorine) bonds, pie-pie stacking, amide-pie stacking, alkyl interactions, and pie-alkyl interactions with LEU'774 (3.13), TRP'777, GLN'715, PHE'718, ARG'771, GLY'180, and HIS'179, respectively. NL8 showed interactions via hydrogen bonds, carbon-hydrogen bonds, halogen (fluorine) bonds, and pie-alkyl interactions with ARG'771 (2.70), TYR'716 (3.30), and GLY'180 (3.37), respectively. NL10 interacted through hydrogen bonds, carbon-hydrogen bonds, halogen (fluorine) bonds, pie-sigma interactions, and pie-alkyl interactions with SER'176 (3.69), LEU'175 (2.63), and ARG'172 (3.33), respectively (Table 7 and fig 3)

NL8
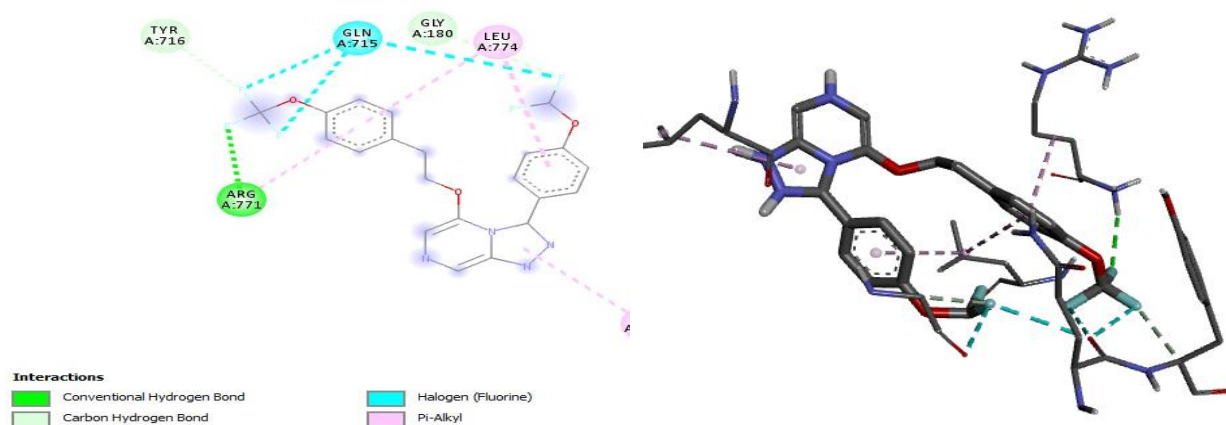
NL9
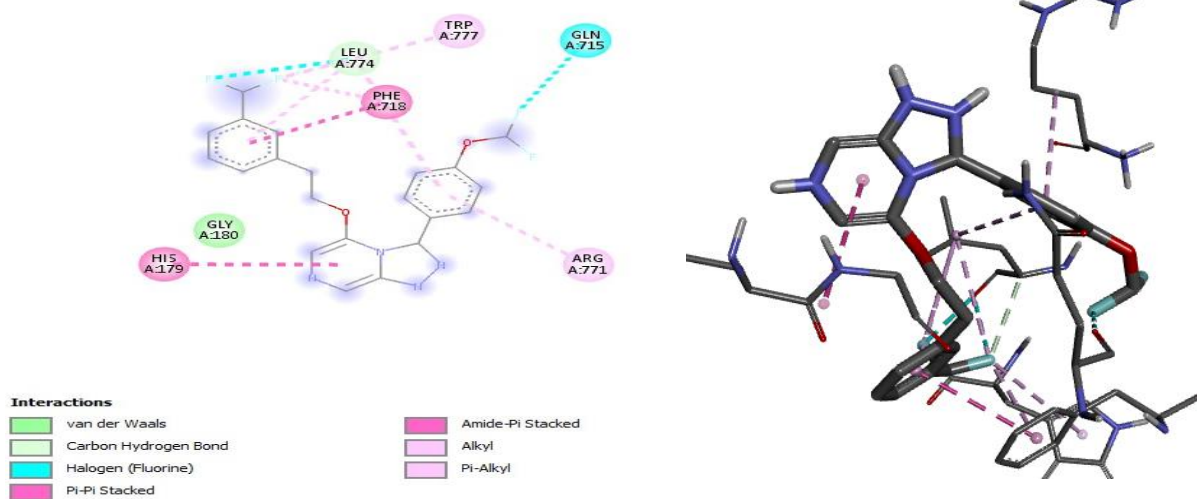
NL10
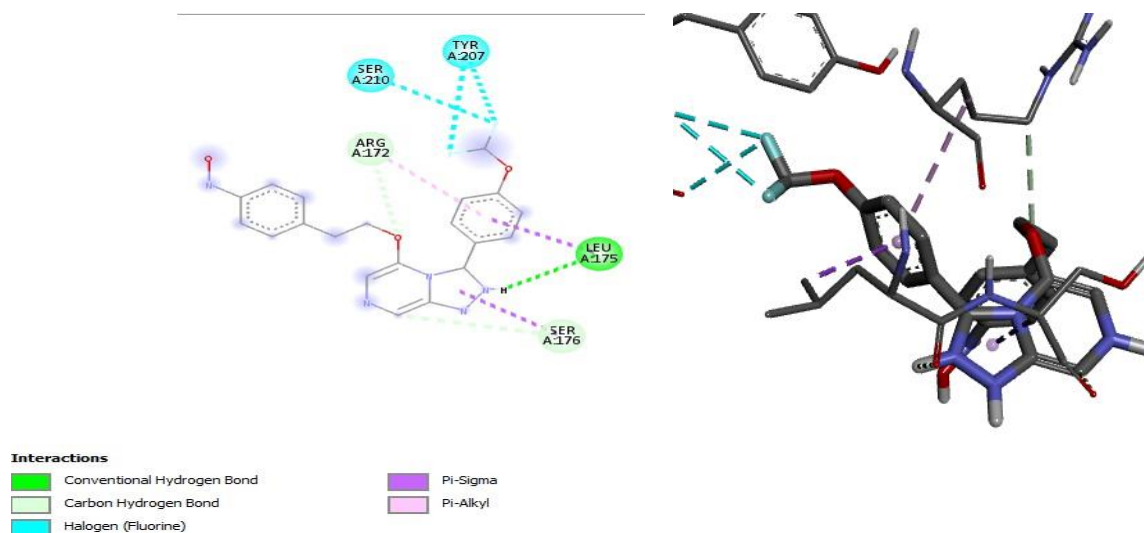
Figure 3: 2D and 3D interactions of NL compounds with 6YCX

Table 7: Binding Affinity and non-bonding interactions of 6YCX Receptor with the Ligands and selected standard drugs

Ligand	Binding affinity (ΔG, kcal/mol)	6YCX Receptor amino acids forming H bond with ligands (H-Bond Distance, Å)	Electrostatic/ Hydrophobic Interactions	IC_{50}
NL7	-8.3	GLN'715(2.71), LEU'175(2.81), ARG'155(2.32)	TYR'716, LEU'774ARG'771, GLY'180, HIS'179, LEU'774, ARG'172, GLN'715	0.46

NL8	-8.9	ARG'771(2.70), TYR'716(3.30), GLY'180(3.37),	LEU'175, LEU'774, GLN'715,	0.39
NL9	-9.3	LEU'774(3.13)	TRP'777, GLN'715, PHE'718, ARG'771, GLY'180, HIS'179,	0.34
NL10	-8.8	SER'176(3.69), LEU'175(2.63), ARG'172(3.33),	TYR'207, SER'210,	0.44
NL18	-8.0	ARG'706(2.18), LEU'698(2.91), GLN'760(2.73), VAL'501(3.29),	GLU'505, VAL'131, LEU'701, PRO'132,	0.40
NL19	-7.8	ASN'177(2.68,2.82), GLN'760(2.77), LEU'698(2.62)	PRO'132, LEU'701, GLU'505, VAL'131	0.77
ARTESUNATE	-7.7	VAL'604(2.34), LYS'634(2.40), SER'639(2.21), ALA'636(1.77)	ILE'635, LEU'599, VAL'430	
PUROMYCIN	-7.9	GLU'660(2.12,2.35), ASN'177(2.57), PRO'661(3.61), THR'569(3.53,3.64),	GLU'173	
PYRIMETHAMINE	-6.6	GLN'203(2.11), TYR'127(2.75), GLY'196(2.70),	PRO'139, ALA'774,	

* Experimental IC50 for the drugs

3.4 Docking Study for Proposed Compound for *Plasmodium Falciparum* (6YCY)

The docking results and interactions of the proposed (3-[4-(Difluoromethoxyl) phyenyl]-5-(2-phenylethoxy) [1,2,4] triazolo [4,3-a] pyrazine hybrids with *Plasmodium Falciparum* (6YCY) are presented in Table.8. The binding affinities (kcal/mol) are (-8.9) NL7, (-8.4) NL8, (-9.3) NL9, (-8.6) NL10, (-9.0) NL18, and standard drugs (-7.5) Artesunate, (-8.2) puromycin and (-6.4) Pyrimethamine. Furthermore, NL7 showed hydrogen bond interaction with THR'10 (1.99), GLU'671 (2.04) and HIS'688 (3.34); TYR'705 (3.29,3.31), ALA'763 (2.83), ARG'706 (2.62), ARG'699 (2.92) and ASN'106 (2.36) for NL8; ASN'242 (2.25,2.58), LYS'197 (2.35), GLY'194(2.49) and GLY'196 (2.57) for NL9; GLU'6 (2.39), THR'4 (2.34) and GLU'671 (1.96); ASP'142 (3.03), THR'146 (2.85), GLN'203 (2.89), ASN'242 (2.56,2.63) and GLY'194 (2.44) for NL18; and GLN'760 (2.29) and LYS'764 (3.21) for L19 as showed Table 8 and Figure 4

Table 8: Binding Affinity and non-bonding interactions of 6YCY Receptor with the Ligands and   selected standard drugs

Ligand	Binding affinity (ΔG, kcal/mol)	6YCY Receptor amino acids forming H bond with ligands (H-Bond Distance, Å)	Electrostatic/ Hydrophobic Interactions
NL7	-8.9	THR'10(1.99), GLU'671(2.04), HIS'688(3.34)	ILE'587, VAL'475, GLU'6, GLU'7, ILE'685, ALA'689
NL8	-8.4	TYR'705(3.29,3.31), ALA'763(2.83), ARG'706(2.62), ARG'699(2.92), ASN'106(2.36)	GLY'103, ASP'101, SER'704, THR'767, LYS'764, TYR'705
NL9	-9.3	ASN'242(2.25,2.58), LYS'197(2.35), GLY'194(2.49), GLY'196(2.57),	ILE'137, ALA'136, ILE'126, ALA'200, CYS'666, ASN'244, PRO'139,
NL10	-8.6	GLU'6(2.39), THR'4(2.34), GLU'671(1.96)	THR'10, VAL'475, LYS'682, ILE'685, GLU'192, GLU'7, LYS'477,
NL18	-9.0	ASP'142(3.03), THR'146(2.85), GLN'203(2.89), ASN'242(2.56,2.63), GLY'194(2.44), GLY'196(2.61), LYS'197(2.38)	GLY'144, PRO'139,
NL19	-7.6	GLN'760(2.29), LYS'764(3.21)	ALA'763, GLN'700, ARG'699,
ARTESUNATE	-7.5	ASN'145(2.61), GLN'203(2.53), LEU'143(2.72), PRO'139(3.08), GLY'196(3.65), ASN'138(3.71)	TYR'140,
PUROMYCIN	-8.2	ASN'145(3.03,3.19), ASN'242(2.78),	ASN'243, VAL'326

		GLY'196(2.96), ASN'138 (1.99	
PYRIMETHAMINE	-6.4	GLN'760(2.57), ASN'106(2.75), LEU'105(2.64,2.09)	GLN'700, TYR'705

NL7
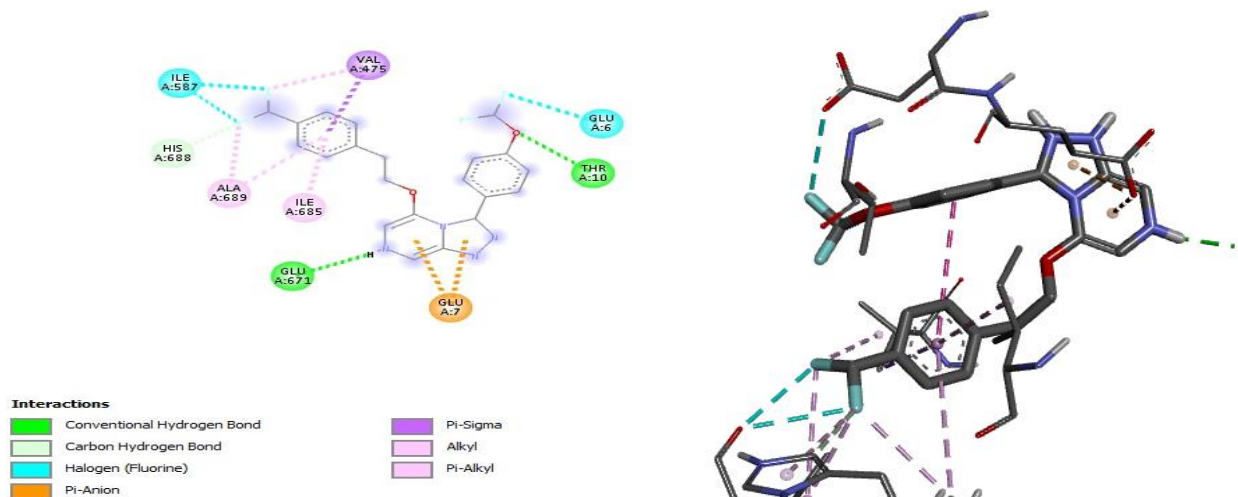
NL9
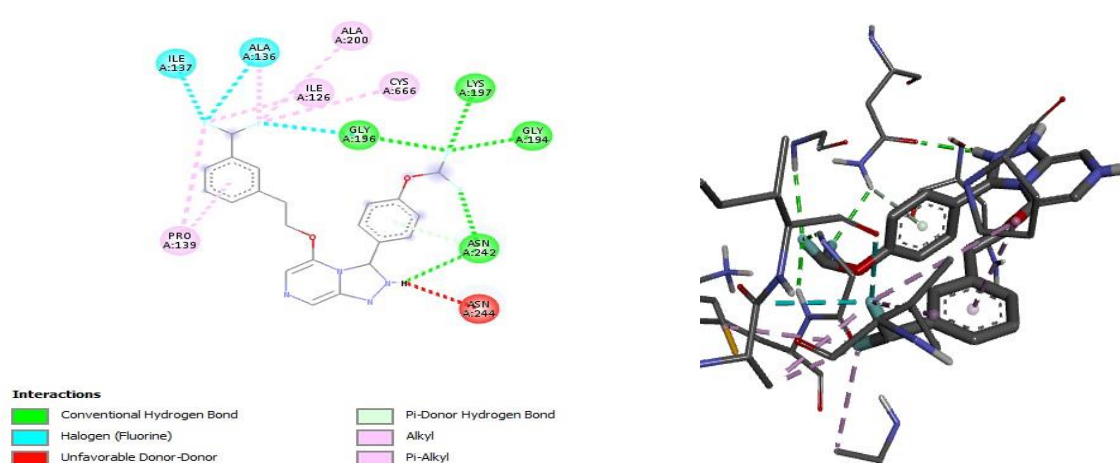
NL18

Figure 4: 2D and 3D interactions of NL compounds with 6YCY

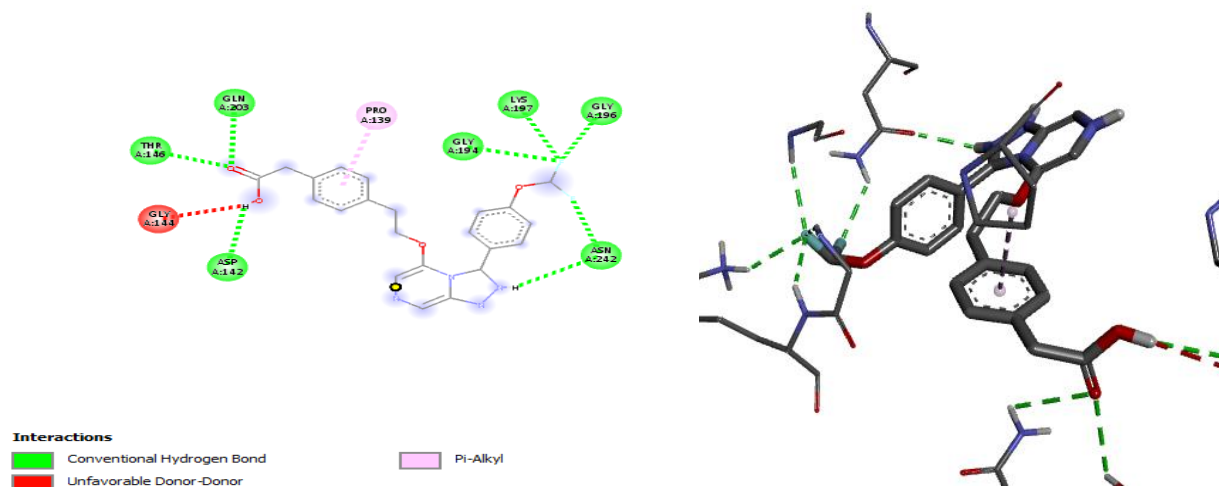## 3.5 Binding Affinity and non-bonding interactions of 6YCZ Receptor with the Ligands and   selected standard drugs

The inhibition constant (Ki, µM) of the new ligand were (0.83) NL7, (0.36) NL8, (0.70) NL9, (1.38) NL10, (0.25) NL18 and (1.63) NL19 indicating that they all bioactive inhibitor of 6YCZ. The docking results showed that NL18 presented highest binding affinity of -9.0 kcal/mol, then NL8 (-8.8 kcal/mol), and NL9 (-8.4 kcal/mol) as displayed in Table 9. Furthermore, NL7 formed hydrogen bond interaction with SER'704 (2.13), GLN'700 (3.08), ASN'106 (2.68), TYR'716 (3.05) and ALA'763 (2.89); NL8 formed hydrogen bond interaction with LYS'673 (2.89), ASN'243 (1.96), ASP'142 (2.80), ASN'138 (1.52), and GLY'203 (3.27); NL9 formed hydrogen bond interaction with ALA'763 (2.33, 3.33), TYR'716 (3.06), ASN'106 (2.64), SER'704 (2.52), ARG'706 (2.32), TYR'705 (3.20, 3.51) and GLN'700 (3.52); NL10 formed hydrogen bond interaction with ASN'106 (2.06), TYR'716 (2.75) and ALA'763 (2.16); NL18 displayed hydrogen bond, Halogen, Pi-cation and pi-anion interactions with GLU'273 (3.30), GLN'280 (3.45) and SER'275 (2.49); and NL19 displayed hydrogen bond, Halogen, unfavourable-Donor-Donor   and Pi- Alky interaction with SER'704 (2.45,2.79), ARG'706 (2.83), ALA'763 (2.62) and TYR'716 (2.62) in Table 9 and Figure 5.

Table 9: Binding Affinity and non-bonding interactions of 6YCZ Receptor with the Ligands and selected standard drugs

Ligand	Binding affinity (ΔG, kcal/mol)	6YCZ Receptor amino acids forming H bond with ligands (H-Bond Distance, Å)	Electrostatic/ Hydrophobic Interactions
NL7	-8.3	SER'704(2.13), GLN'700(3.08), ASN'106(2.68), TYR'716(3.05), ALA'763(2.89),	TYR'705, ARG'706, ARG'699, LYS'764

NL8	-8.8	LYS'673(2.89), ASN'243(1.96), ASP'142(2.80), ASN'138(1.52), GLY'203(3.27)	TYR'140, LYS'141, PRO'139, GLN'203,
NL9	-8.4	ALA'763(2.33,3.33), TYR'716(3.06), ASN'106(2.64), SER'704(2.52), ARG'706(2.32), TYR'705(3.20,3.51), GLN'700(3.52),	ARG'699, LYS'764, TYR'705, ALA'763,
NL10	-8.0	ASN'106(2.06), TYR'716(2.75), ALA'763(2.16),	LYS'764, TYR'716, ALA'763, ARG'706
NL18	-9.0	GLU'273(3.30), GLN'280(3.45), SER'275(2.49),	ARG'247, GLU'474, LEU'271, LEU'272
NL19	-7.9	SER'704(2.45,2.79), ARG'706(2.83), ALA'763(2.62), TYR'716(2.62)	ARG'699, ARG'706, ALA'763
ARTESUNATE	-8.0	ASN'138(2.10), GLY'196(2.61),	PRO'139,
PUROMYCIN	-8.3	GLU'199(2.40), LYS'202(2.49), THR'198(2.20), PRO'229(3.10), ASN'242(2.48)	
PYRIMETHAMINE	-6.7	GLU'406 (2.46,2.56), ILE'409(2.82),	VAL'411, TRP'423, ARG'606, LYS'634

NL8
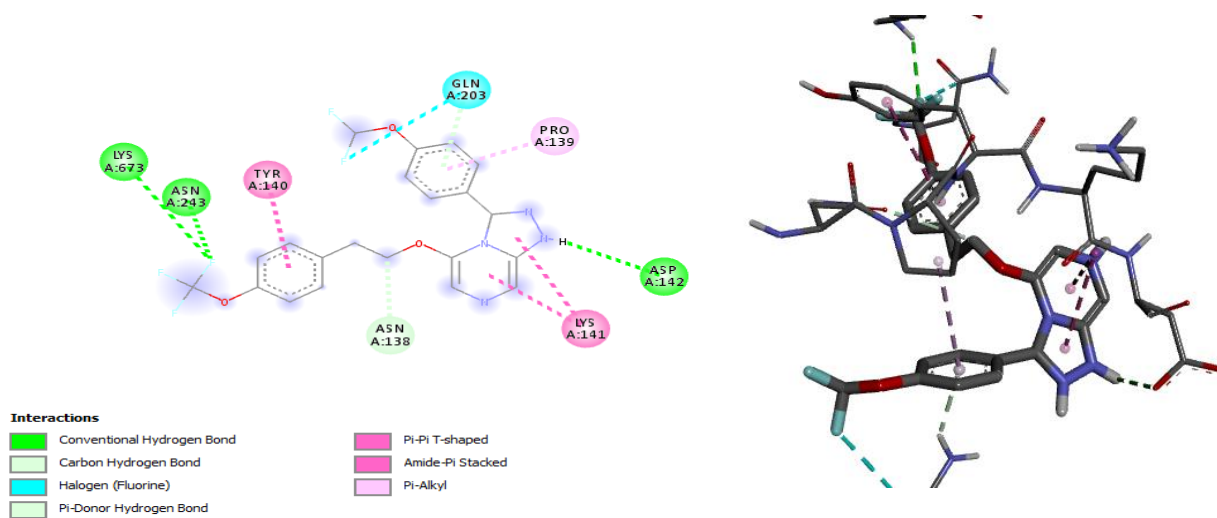
NL9
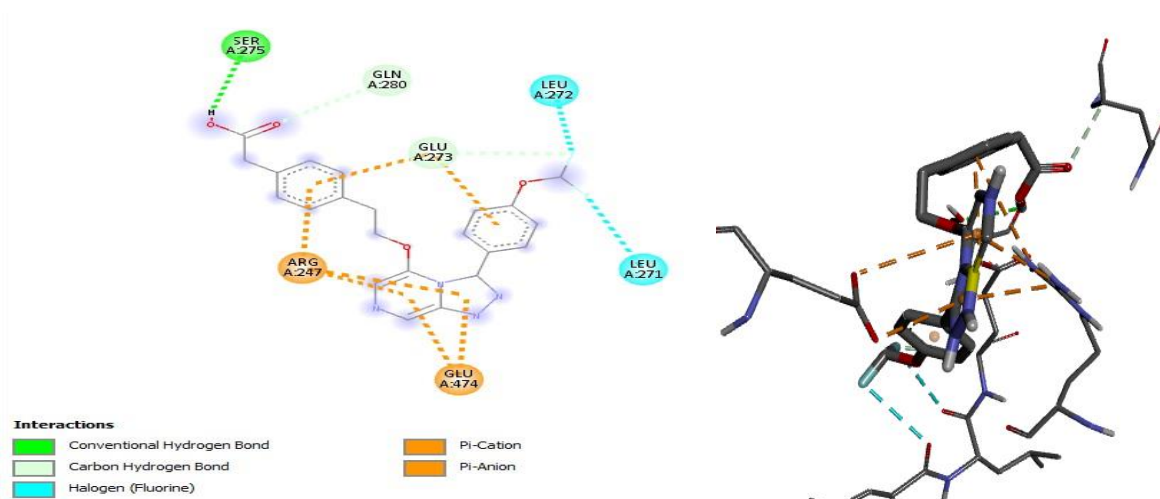
NL18

Figure 5: 2D and 3D interactions of the new compounds with 6YCZ

4.7.3 ADMET properties of the predicted 1,2,4 – triazolo[4,3-α] pyrazine compounds
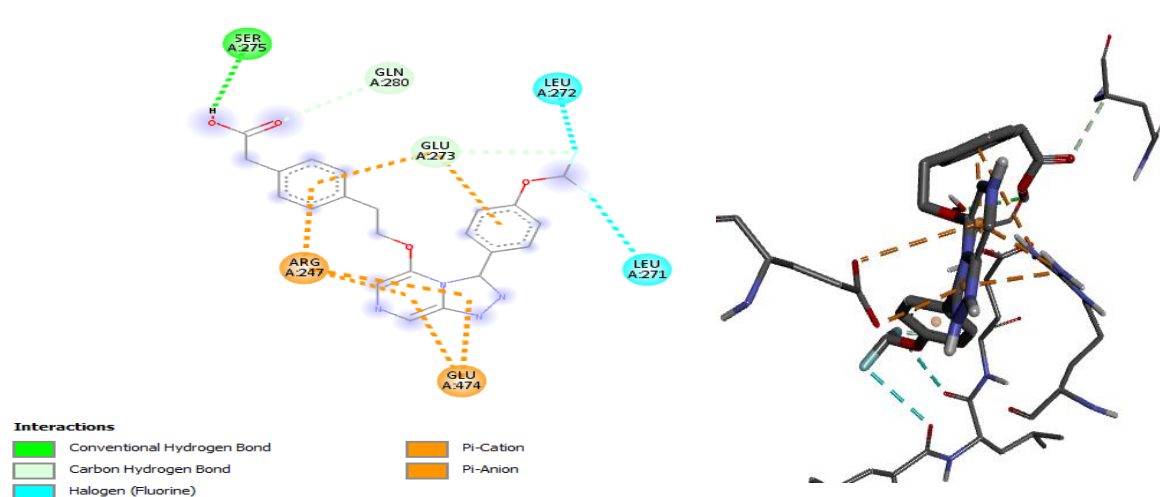
Table 10 shows the ADMET properties of the predicted 1,2,4–triazolo[4,3-α] pyrazine ligands, that is NL7, NL8, NL9, NL10, NL18, NL19 three standard drugs (Artesunate, Puromycin and Pyrimethamine). All the new ligands displayed good medications through the oral absorptivity of H_2O solubility, $CaCO_2$ Permeability and Skin permeability. P-glycoprotein, also known as P-gp, is largely utilized to eliminate extraneous components from the central nervous system to prevent the buildup of extraneous materials in cells, particularly medications [25]. Therefore, all ligands are P-glycoprotein substrates also, the ligands and the standard drugs are P-glycoprotein inhibitors. The ligands can pass the blood-brain barrier (BBB), but their permeability is high, indicating a low distribution to the central nervous system. All the ligands, Puromycin and Pyrimethamine are CYP3A4 substrates, which means they can be metabolized and eliminated from the body. NL10, NL18, NL19 as well as the standard drugs are CYP1A2 inhibitor, CYP1A2 Substrate which means they might be the drug metabolic block activity of the CYP1A2 enzyme, potentially increasing drug quantities in the body There are numerous common genetic variants that alter the expression of the CYP2C19 gene, which changes enzyme activity in the metabolic pathways of medicines containing this enzyme. Therefore, NL10, NL18 and NL19 are inhibitory of . Ligands NL7, NL8, NL9, NL18, NL19 and Artesunate block the ether-a-go-go gene (hERG I), which can results heart failure [26]. The Ames test is an experiment that determines a chemical's or drug's capacity to produce DNA mutations. This test is based on the premise that DNA is chemically equal in different living creatures, hence malaria can be utilized to discover possible human carcinogens more efficiently. Moreso, NL7, NL8 NL9, NL18 and NL19 are not AMES toxicity. The new ligands and two standard drugs that is NL10, NL18, NL19, Artesunate and Pyrimethamine are non-hepatotoxic and all ligands are Skin sensitization proposed by extended stability in the body and enhanced drug effectiveness.

Table 10: ADMET properties of the predicted 1,2,4 – triazolo[4,3-α] pyrazine compounds

Property	Model Name	NL7	NL8	NL9	NL10	NL18	NL19	ARTESU	PUROMY	PRIYM
ABSORBTION	H_2O solubility	-5.81	-6.09	-5.74	-5.19	-4.49	-5.36	-2.92	2.14	-0.67
	$CaCO_2$ Permeability	-4.90	-5.02	-4.89	-5.38	-4.98	-4.76	-4.73	-6.41	-5.92
	Intestinal absorption (human)	YES	YES	YES	YES	YES	YES	YES	NO	YES
	Skin permeability	-3.77	-3.77	-3.82	-3.05	-2.88	2.78	2.29	7.73	0.45

	P-glycoprotein substrate	NO	NO	NO	NO	NO	NO	NO	YES	YES
	P-glycoprotein I inhibitor	NO	NO	NO	NO	NO	NO	NO	NO	NO
DISTRIBUTION	*VDSS (human)	2.35	2.64	2.37	0.81	0.69	1.26	1.21	0.55	2.62
	Fraction on bound (human)	1.68	1.87	1.73	1.72	2.14	1.69	0.61	0.35	0.5
	BBB permeability	YES	YES	YES	YES	YES	YES	NO	NO	YES
	*CNS permeability	-2.75	-2.75	-2.78	-2.05	-2.65	-2.57	-3.55	-3.98	-3.35
METABOLISM	CYP1A2 inhibitor	YES	YES	YES	NO	NO	NO	NO	NO	NO
	CYP1A2 Substrate	NO	YES	NO	NO	NO	NO	NO	NO	NO
	CYP2C19 inhibitor	YES	YES	YES	NO	NO	NO	NO	NO	NO
	CYP2C19 substrate	NO	NO	NO	NO	NO	NO	NO	YES	NO
	CYP2C9 inhibitor	YES	YES	YES	YES	YES	YES	NO	NO	NO
	CYP2C9 substrate	YES	YES	YES	YES	YES	YES	NO	NO	NO
	CYP2D6 inhibitor	NO	NO	NO	NO	NO	NO	NO	NO	NO
	CYP2D6 substrate	NO	NO	NO	NO	NO	NO	NO	NO	NO
	CYP3A4 inhibitor	YES	NO	YES	YES	NO	YES	NO	NO	NO
	CYP3A4 substrate	NO	NO	NO	NO	NO	NO	YES	NO	NO
EXCREATION	Total clearance	9.19	8.13	9.23	6.69	4.34	5.85	12.92	1.97	7.45
	Renal OCT2 substrate	NO	NO	NO	NO	NO	NO	NO	NO	NO
TOXICITY	AMES toxicity	NO	NO	NO	YES	NO	NO	YES	YES	YES
	Max. tolerated dose (human)	0.90	0.88	0.88	0.39	-0.01	0.45	-0.91	1.00	0.18

Bioconcentration factor	1.58	1.82	1.63	1.34	0.58	1.52	-1.14	-4.26	-1.37
hERG I inhibitor	YES	YES	YES	NO	YES	YES	YES	NO	NO
Oral- Rat Acute toxicity (LD$_{50}$)	2.49	2.54	2.48	2.51	2.54	2.43	3.26	2.70	2.63
Oral- Rat Chronic toxicity (LOAEL)	0.76	0.57	0.75	0.91	1.25	0.99	2.31	0.88	1.69
Hepatotoxicity	YES	YES	YES	NO	NO	NO	NO	YES	NO
Skin sensitization	NO	NO	NO	NO	NO	NO	YES	YES	YES
T. Pyriformis toxicity	-76.29	-153.60	-75.72	-52.09	-121.20	-27.97	-10.16	-314.00	1.07
Minnow toxicity	6.04	6.39	6.03	6.02	5.76	5.86	3.48	2.62	4.12

CONCLUSION

In this paper, new 1,2,4-triazolo[4,3-α] pyrazine hybrids were modeled against *Plasmodium falciparum* using density functional theory method, QSAR and molecular docking methods. The developed QSAR models were validated and robust enough to predict the experimental bioactivities of the compounds. More so, the results gotten from docking study predicted stable conformations of the ligands within the *Plasmodium falciparum* active gouge. Further studies should determine, Synthesize and perform in vitro studies of the predicted triazolo[4,3-a] pyrazine-based compounds against *Plasmodium falciparum* to further validate and complement the in-silico findings.

REFERENCES

1   WHO   (2021)? World   Malaria   Report   2021.   Switzerland: World   Health
     Organization. ISBN 978-92-4-   004049-6.

2 Caminade C, Kovats S, Rocklov J, (2014). "Impact of climate change on global malaria
     distribution."Proc Natl Acad Sci U S A,   111(9):3286–3291.

3 Mace, K. E., Arguin, P. M. Lucchi, N. W Tan, K. R. (2019). Surveill. Summ. 68(5), 1.

4 Kondilis E, Giannakopoulos S, Gavana M, Ierodiakonou I, Waitzkin H, Benos A. (2013)
     Economic crisis, restrictive policies, and the population's health and health care: the
     Greek case. *Am J Public Health*;103(6):973–979. doi:10.2105/AJPH.2012.301126

5 Plucinski MM, Talundzic E, Morton L, (2015). Efficacy of artemether-lumefantrine and
     dihydroartemisinin-piperaquine for treatment of uncomplicated malaria in children in
     Zaire and Uíge provinces, Angola. *Antimicrobial Agents Chemother*.;**59**(1):437–443.

6 Reyburn H. (2010). New WHO guidelines for the treatment of malaria. BMJ. 340:c2637. doi:
     10.1136/bmj.c2637.

7 Ramchander, M., Setha, G., Deetic, B. and Kalyani, S. (2015). Synthesis and Biological
     Activities of pyrimidines. A review international *journal of pyarmTech Research*, *8
     (6);88-93*.

8 Alyar, S.N. Karacan, J. (2009) Enzyme Inhibiton. Med. Chem, 24, 4, 986.
     https://doi.org/10.1080/14756360802561220.

9 Sondhi, S.M., Dinodia, M., Rani, R. Shukla, R., and Raghubir, R. (2009). Synthesis, anti-
     inflammatory and analgesic activity of some pyrimidine derivatives, *indiaan journal of
     chemistry B, 48(2); 273-281*.

10 Wood, P.M., Woo, L.W.L., Labrosse J., Trusselle, M.N., Abbate, S. (2008). New
     Trisubstituted 1,2,4-Triazole Derivates as Potent Ghrelien Receptor Antagonists. *J Med
     Chem.,* **51:** 42236-42338

11 Mavrova,A.T., Wesselinova, D., Tsenov,Y.A., Pavletta, d. (2009) Synthesis, cyctotoxicity
     and effects   0f some 1,2,4- Triazole and 1,3,4- thiadiazole derivatives on
     immunocompetent cells. *Eur v J.Med .Chem.,***44**:63-69

12 Sondhi, S.M., Jani, S., Dinodia, M., Shukla, R., and Raghubir, R, (2007). One pot Synthesis
     of pyrimidine and bispyrimidine derivatives and their evaluation for anti-inflammatory
     and analgesic activities. Bio-organic and medicinal chemistry, 15(10);3334-3344

13 Huighes, J. D.; Blagg, J.; Price, D. A.; Bailey, S.; Decrescenzo, G. A.; Devraj, R. V.;
     Ellsworth, E.; Fobian, Y. M.; Gibbs, M. E.; Gilles, R. W.; Greene, N.; Huang, E.;
     Krieger-Burke, T.; Loesel, J.; Wager, T.; Whiteley, L.; Zhang, Y. (2022)
     Physicochemical drug properties associated with in vivo toxicological outcomes.
     Bioorg. Med. Chem. Lett 18, 4872−4875

14 Ferreira SB, Sodero ACR, Cardoso MFC, et al.2010. Synthesis, biological activity, and molecular modeling studies of 1 -1,2,3-triazole derivatives of carbohydrates as alfa-glucosidases inhibitors. J. Med. Chem 2010; 53:2364-75

15 Open-Source Malaria Project Wiki; A new triazolo-pyrazine series for OSM series 4. Availableonline: http://malaria.ourexperiment.org/osdd_malaria_shared/7949/A_New_Triazolopyrazine _Series_for_OSM__Series_4.html (accessed on 20 January 2021)

16 Johnson, D.J.G.; Jenkin, I.D.; Huxley, C.; Coster, M.J.; Lum, K.Y.; Wihite, J.M.; Avery, V.M.; DAvis, R.A (2021). Synthesis of New Triazolo pyridazine Antimalarial compounds. Molecules,26, 2421.https://doi.org/10.3390/molecules26092421

17 Semire, B., & Odunola, O. A. (2019). Density Functional Theory (DFT) Study on α, α-Bis (2-benzothiophen-1-yl)-4H-cyclopenta [2, 1-b, 3; 4-b′] dithiophene Derivatives for Optoelectronic Devices. *A A*, 1(2), 3.

18 Semire B.; Oyebamiji, A.; Ahmad, M. (2012): Theoretical Study on structure and Elctronic Properties of 2,5- Bis [4-N, N- Diethylaminostyl] Thiophene and its furan and pyrrole Derivatives Using Density Functional Theory. *Pakistan Journal of Chemistry*, 2(4), 166-173

19 Rivera-Delgado, E., Xin, A., & Von Recum, H. A. (2019). Using QSARs for predictions in drug delivery. *bioRxiv (Cold Spring Harbor Laboratory)*. https://doi.org/10.1101/727172

20 Oyebamiji Abel Kolawole and Semire Banjo (2016). DFT-QSAR model and docking studies of antiliver cancer (HEPG-2) activities of 1, 4-Diydropyridine based derivatives, Cancer Biology, 6(2):69-78. Impact Factor: 0.654 | Publisher: Marsland Press. Website: http://www.sciencepub.net

21 Abdullahi, M., & Adeniji, S. E. (2020). In-silico molecular docking and ADME/pharmacokinetic prediction studies of some novel carboxamide derivatives as anti-tubercular agents. Chemistry Africa, 3(4), 989-1000.

22 Veerasamy, R., Rajak, H., jain, A., Sivadasan, S., Varghese, CP., Agrawal,R.K.,(2011).Validation of qsar models-strategies and importance. Int.j. Drug Des. Discov.3,511-519.

23 Ameji, J. P., Uzairu, A., Shallangwa, G. A., & Uba, S. (2023). Design, pharmacokinetic profiling, and assessment of kinetic and thermodynamic stability of novel anti-Salmonella typhi imidazole analogues. *Bulletin of the National Research Centre*, *47*(1), 1-12.

24 Miar, M., Shiroudi, A., Pourshamsian, K., Oliaey, A. R., & Hatamjafari, F. (2021). Theoretical investigations on the HOMO–LUMO gap and global reactivity descriptor studies, natural bond orbital, and nucleus-independent chemical shifts analyses of 3-

phenylbenzo [d] thiazole-2 (3 H)-imine and its para-substituted derivatives: Solvent and substituent effects. *Journal of Chemical Research*, *45*(1-2), 147-158.

25 Adegbola P.I., Semire B., Fadahunsi O.S. and Adegoke A.E., (2021) Molecular docking and ADMET studies of Allium cepa, Azadirachta indica and Xylopia aethiopica isolates as potential anti-viral drugs for Covid-19. VirusDisease. https://doi.org/10.1007/s13337-021-00682-7

26 Gualdani R, Tadini-Buoninsegni F, Roselli M, Defrenza I, Contino M, Colabufo NA, Lentini G. (2015) Inhibition of hERG potassium channel by the antiarrhythmic agent mexiletine and its metabolite m-hydroxymexiletine. *Pharmacol Res Perspect*; **3**(5): -00160. Doi: 10.1002/prp2.160.